Available online at www.sciencedirect.com
ScienceDirect
Journal of the European Ceramic Society 32 (2012) 495–502
www.elsevier.com/locate/jeurceramsoc

Dislocation microstructure of 4H–SiC single crystals plastically deformed around the transition temperature

A. Lara, M. Castillo-Rodríguez, A. Muñoz, A. Domínguez-Rodríguez *

Departamento de Física de la Materia Condensada, Facultad de Física, Universidad de Sevilla, Apartado 1065, 41012 Sevilla, Spain

Received 16 February 2011; received in revised form 26 July 2011; accepted 6 August 2011
Available online 4 September 2011

Abstract

4H–SiC specimens were plastically deformed by basal slip at temperatures between 800 °C and 1300 °C. Samples were investigated by means of transmission electron microscopy and high-resolution techniques. The accepted transition temperature (1030 °C) was found not to be actually so well defined since the two mechanisms were operating together between 1000 °C and 1100 °C. Dissociation of basal dislocations takes place over the entire temperature range investigated, having a different influence on each regime. In the high temperature regime, after dissociation the two partials slip together in the basal plane fringing a stacking fault. We have determined the dissociation width, obtaining a stacking fault energy of 20 ± 5 mJ/m^2. However, below the transition temperature the difference in mobility of the partials and the low stacking fault energy allow the leading partial to glide alone. We discuss the consequences of this finding for the crystal structure (cubic bands nucleation) and mechanical behaviour (high work-hardening rate).

Keywords: D. SiC; B. Electron microscopy; C. Mechanical properties; Dislocations

1. Introduction

The advanced ceramic SiC is currently of great interest due to its excellent physicochemical properties such as resistance to erosion and corrosion, high thermal conductivity, small expansion coefficient, low density, and hardness second only to diamond. This polycrystalline material is widely used in industry as an abrasive (grinding, sanding, etc.), for refractory products (bricks, crucibles, etc.), and as a structural material in the manufacture of such products as bearings, valves and resistors. Moreover, recent advances providing precise knowledge of its crystal structure together with developments in the physics of electronics endow this material with a promising future in functional applications as well. In particular its properties as a wide band gap semiconductor[1] make it a good candidate for the manufacture of electronic devices that are operative at high temperatures and in harsh environments – conditions under which it is impossible to use other semiconductor materials such as Si or GaAs.

The existence of numerous polytypes of this material makes it even more interesting theoretically and technologically. Indeed, there have been several studies aimed at providing a theoretical explanation of the occurrence of polytypism in SiC,[2–4] in particular that a local transformation inside the matrix may affect the material's initial properties.[5–11] This transformation had been observed in a 4H–SiC single crystal polytype during different processes: (i) thermal oxidation,[12] (ii) annealing in Ar for 90 min at 1150 °C,[13] and (iii) stress induced at temperatures between 400 °C and 700 °C.[14] In all cases, transmission electron microscopy revealed stacking faults and local bands of 3C polytype in the 4H–SiC matrix. The occurrence of this phenomenon strongly affects the plasticity of this material which, as described by Demenet et al.[15] exhibits two regimes of different mechanical behaviour separated by a transition temperature T_c of about 1030 °C.

We have investigated the mechanical properties of 4H–SiC by means of compression tests which provided information on the activation energy of each mechanism. Our results confirmed the findings of Demenet et al.[15] of the existence of a transition temperature. The main focus of this work is the analysis of specimens after deformation by means of weak-beam dark-field (WB-DF) imaging and high-resolution TEM (HRTEM) observa-

* Corresponding author. Tel.: +34 954557849.
E-mail address: adorod@us.es (A. Domínguez-Rodríguez).

0955-2219/$ – see front matter © 2011 Elsevier Ltd. All rights reserved.
doi:10.1016/j.jeurceramsoc.2011.08.016

tions to gain insight into the deformation mechanism operating in each regime.

2. Experimental procedure

The crystals used in this work were provided by *Sterling Semiconductor, Inc.* (*USA*) as cylinders 5 cm in diameter, grown by the physical vapour transport (PVT) technique along the [0 0 0 1] direction. The as-received crystals were oriented using the Laue X-ray back-reflection technique. The specimens for mechanical tests were cut in the form of parallelepipeds of 2.7 mm × 2.7 mm × 5.5 mm using a low-speed diamond saw, and each lateral face was polished with diamond pastes down to 3 μm in grain size. Specimens were oriented to favour the activation of only one $(0\,0\,0\,1)1/3\langle\bar{1}\,2\,\bar{1}\,0\rangle$ basal slip system with a Schmid factor of $f_s = 0.5$, where two lateral faces of the sample are parallel to the $\{\bar{1}\,0\,1\,0\}$ plane and the compression axis lies in this plane, at 45° from the [0 0 0 1] direction. Deformation tests were performed in air at temperatures between 800 °C and 1300 °C at cross-head speeds of 5 and 10 μm/min, corresponding to initial strain rates of $\dot{\varepsilon} = 1.5 \times 10^{-5}\ s^{-1}$ and $\dot{\varepsilon} = 3.0 \times 10^{-5}\ s^{-1}$ in an Instron machine, model 1185.

Since the transition temperature is around 1000 °C, we selected 4H–SiC specimens deformed at 900 °C, 1000 °C, 1100 °C, and 1300 °C to prepare the TEM specimens. Foils were cut parallel to the basal slip plane for weak-beam dark-field (WB-DF) imaging, and parallel to the $(\bar{2}\,1\,1\,0)$ plane to perform high-resolution TEM (HRTEM) observations. All foils were mechanically ground to a thickness of about 100 μm and polished with diamond paste of grain size 3 μm. They were then dimpled to ∼30 μm (*Dimpler grinder Gatan Model-656*) and ion beam thinned to electron transparency (*PIPS Gatan Model-691*). A thin carbon coat was deposited onto the WB-DF foils by vacuum evaporation to prevent charge build-up during observation in the electron microscope (this was not done for the HRTEM foils since even a thin carbon coat would have made it difficult to observe Si and C atom columns in the specimens). For WB-DF, the dislocation microstructure was examined using a Philips CM200 microscope operating at 200 kV, which allows large tilts. For HRTEM, a JEOL JEM-4000EX microscope with a point resolution of 0.17 nm was used, operating at 400 kV.

3. Results and discussion

Mechanical tests reveal that 4H silicon carbide deformed by basal slip presents a transition temperature T_c between 1000 °C and 1100 °C that separates two regimes of clearly different mechanical behaviours (Fig. 1). This transition had previously been described by Samant et al. in 6H–SiC[3,5] and confirmed in a more detailed investigation of the transition temperature in 4H–SiC by Demenet et al.[15]. Since plastic deformation of single crystals is due to the movement of dislocations, we studied the dislocation microstructure to try to gain insight into the mechanical behaviour of this material. This study involved two complementary techniques of transmission electron microscopy (TEM), for one hand, the weak beam technique to study the general organization of the dislocations in their slip plane, and

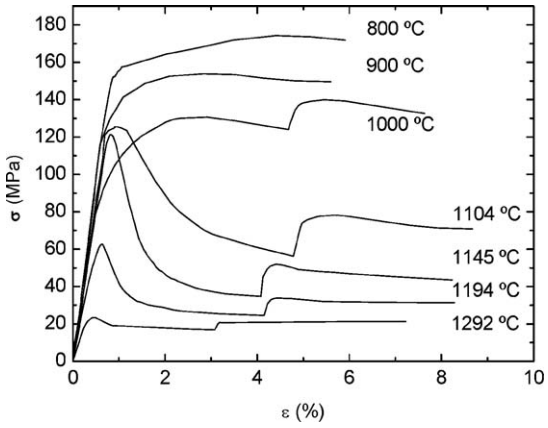

Fig. 1. Engineering stress–strain curves of the 4H–SiC samples deformed at various temperatures at a strain rate of $\dot{\varepsilon} = 1.5 \times 10^{-5}\ s^{-1}$. For $T \geq 1000$ °C, the strain rate was jumped up to $\dot{\varepsilon} = 3.0 \times 10^{-5}\ s^{-1}$ until $\varepsilon \sim 4\%$.

on the other, high resolution transmission electron microscopy (HRTEM) to examine configurations at the atomic scale such as possible changes in the stacking plane sequence, and to study the dislocation core. We selected specimens deformed at temperatures above (1300 °C), below (900 °C), and close to (1100 °C and 1000 °C) the transition temperature.

3.1. Above the transition temperature

Fig. 2 shows the microstructure of dislocations of a specimen deformed by basal slip at 1300 °C. From the diffraction pattern at the bottom, one readily observes that the dislocation lines are arranged along simple crystallographic directions, indicating that the Peierls mechanism controls dislocation glide. Also, the

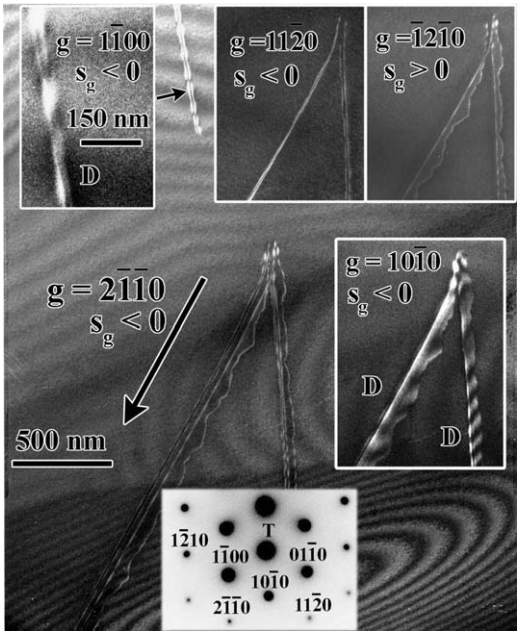

Fig. 2. Dislocation microstructure of 4H–SiC deformed by basal slip at 1300 °C. Insets taken under different *g* reflections show the stacking fault fringes and the extinction of each partial.

Table 1
Distance d between partial dislocations for various electron beam orientations θ (angle between the electron beam and [0 0 0 1] direction) of the basal dissociated dislocations 1 and 2 in Fig. 3.

Dissociated dislocation 1	θ (°)	5 ± 2	15 ± 2	25 ± 2	35 ± 2	−8 ± 2	−18 ± 2	−28 ± 2
	d (nm)	32 ± 2	28 ± 2	26 ± 2	23 ± 2	31 ± 2	27 ± 2	25 ± 2
Dissociated dislocation 2	θ (°)	5 ± 2	15 ± 2	25 ± 2	35 ± 2	−8 ± 2	−18 ± 2	−28 ± 2
	d (nm)	33 ± 2	29 ± 2	28 ± 2	27 ± 2	33 ± 2	29 ± 2	27 ± 2

basal dislocations are dissociated into two partials fringing a stacking fault (SF) according to:

$$1/3\langle \bar{1}\,2\,\bar{1}\,0\rangle \rightarrow 1/3\langle \bar{1}\,1\,0\,0\rangle + \mathrm{SF} + 1/3\langle 0\,1\,\bar{1}\,0\rangle \quad (1)$$

At the top of the figure, there is a basal dissociated dislocation which is isolated, i.e., it does not form a dipole with another dislocation. The inset on the left shows the fringes coming from the stacking fault (since $\mathbf{g}\cdot\mathbf{b}$ is not an integer). In this configuration, the partials are quite straight and their separation of about 30 nm remains almost constant (see also the partials of Fig. 3). However, in the centre of Fig. 2 one observes pairs of partials forming dipoles. The stacking fault displays fringes in the inset on the right. Moreover, the insets at the top centre and right taken under different g reflections show each partial's intensity extinction, and reveal that in this configuration one pair of partials has straight dislocation lines separated by 50 nm, which is somewhat larger than in the isolated case. The situation for the other pair of partials is different: one is straight but its pair zigzags, producing a major fluctuation of the dissociation width of between 50 and 115 nm. This difference could be due to the combination effect between Peierls barrier and dipolar interactions.

The stacking fault plane seems to be close to the basal plane since, with tilting around the dislocation line, it was observed that the dissociation width decreases as soon as the basal plane is left. To further characterize this material's dissociation properties, we determined the stacking fault habit plane and the dissociation width for the two pairs of partials in Fig. 3. This was done by tilting around the direction of the dislocation line, which coincides with $\mathbf{g} = 1\,\bar{2}\,1\,0$, and taking micrographs at different orientations. Taking into account the angle of tilt at the microscope, and using Wulff's network together with a stereographic projection, we determined the angle θ between the electron beam and the [0 0 0 1] direction for each orientation. We also measured the dissociation distance d between the images of the two partial dislocations. Note that this distance d is not the real distance between partials, but the distance between partials projected onto the plane perpendicular to the electron beam. It needs to be emphasized that the dislocation signal originates from a region in the vicinity of the core that is appropriately distorted to satisfy the Bragg orientation, away from the actual dislocation line position. Furthermore, since the partials have non-parallel Burgers vectors, they are viewed under distinct $\mathbf{g}\cdot\mathbf{b}$ conditions and their images are thus shifted differently with respect to the actual positions of the partials, depending on the sign of the product $s_g\,\mathbf{g}\cdot\mathbf{b}$. This property contributed the greatest uncertainty to the calculation of the stacking fault habit plane and the dissociation width.

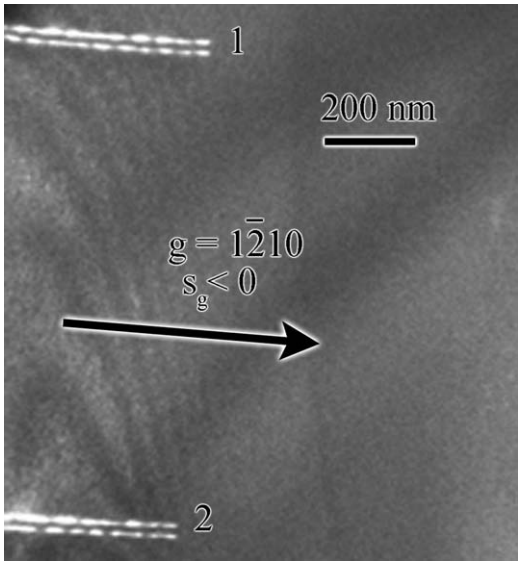

Fig. 3. TEM micrograph of 4H–SiC deformed by basal slip at 1300 °C, showing the two basal dissociated dislocations that were analyzed.

Table 1 lists the distances d between the images of partials for various electron beam orientations θ, corresponding to the two dissociated basal dislocations in Fig. 3.

The real dissociation width h and the angle β between the stacking fault habit plane and the [0 0 0 1] direction are related to d and θ by the following expression[16]:

$$\cos\left(\arccos\left(\frac{d}{h}\right) + \beta\right) = \sin\ \theta \quad (2)$$

Then, a least-squares fit of expression (2) to the various (θ_i, d_i) pairs measured experimentally yields the values of β and h (Table 2). In both cases, the stacking fault habit plane is close to the basal plane with partials separated by 30 nm. Dissociation thus seems to take place by glide. These results are coherent with literature reports.[15]

With the dissociation process characterized and the dissociation width and stacking fault habit plane known, one can now estimate the stacking fault energy γ between partials. The repulsive force between partials is balanced by the stacking fault generated between them. Hence, from their respective

Table 2
Distance h between partials and the angle β between the stacking fault plane and [0 0 0 1] direction of the basal dissociated dislocations 1 and 2 in Fig. 3.

	β (°)	h (nm)
Dissociated dislocation 1	110 ± 15	32 ± 4
Dissociated dislocation 2	100 ± 15	33 ± 4

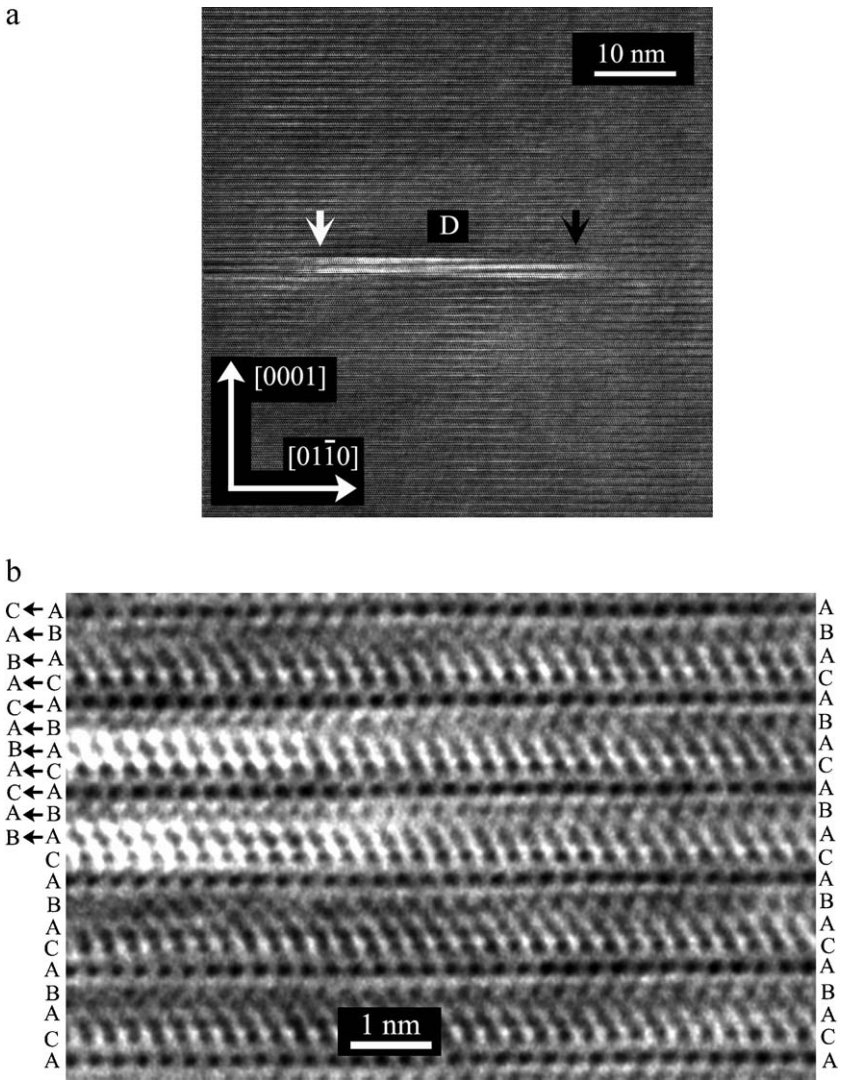

Fig. 4. (a) High resolution micrograph of 4H–SiC deformed by basal slip at 1300 °C. (b) Stacking plane sequence beside the black arrow of Fig. 4a.

expressions,[17] one obtains that the stacking fault energy γ is given by:

$$\gamma = \frac{\mu b^2}{2\pi s}\left(\cos^2[\psi] + \left(\frac{1}{1-v}\right)(\sin^2[\psi] + 2\sin[\psi]\sin[a]\cos[a])\right) \quad (3)$$

where $\mu = 159$ GPa[18] is the shear modulus, v is Poisson's modulus with a value of 0.25, **b** is Burgers vector of the partial dislocation and ψ its character, s is the dissociation width, and α is the angle between the stacking fault plane and the slip plane. Then, considering the two configurations in Fig. 3, where the screw basal dislocations 1 and 2 are glide-dissociated ($\alpha = 0°$) into two partial dislocations ($\psi = 30°$) separated by $s = h = 32 \pm 4$ nm (Table 2), one obtains $\gamma = 20 \pm 5$ mJ/m^2. This value is in good agreement with the literature. Hong et al.[19,20] for instance, reported a value of $\gamma = 14.7 \pm 2.5$ mJ/m^2. Based on a theoretical model (ANNNI), the stacking fault energy should be between 19.1 and 27.2 mJ/m^2.[21,22] The value we obtained is thus satisfactory in the sense that it lies within the error bars of these two determinations.

Fig. 4a is a high resolution micrograph of the 4H–SiC specimen deformed by basal slip at 1300 °C. One observes a bright contrast of about 30 nm in length within the basal plane. This contrast could come from the stacking fault between the partial dislocations at the edges marked by arrows in Fig. 4a. This would be in good agreement with the weak beam results for the dissociation process which showed the dissociation plane to be close to the basal plane (Table 2), and the dissociation width to be approximately 30 nm.

Fig. 4b is a magnification of the zone of the black arrow in Fig. 4a. The projection of a double Si–C column corresponds to a black spot in the {$\bar{2}$ 1 1 0} plane of the micrograph. The resolution of the microscope is insufficient to distinguish between the C and Si atoms. Indeed, as one sees in Fig. 4b, this projection is not spherical in shape, but is elongated due to the overlap of the Si and C atom columns. Depending on their relative positions, they are elongated in one direction or another. The sequence of Si stacking planes in the 4-H structure is . . .CABACABAC. . . in which the repeating sequence involves four planes, and for the case of C is . . .αβγ. . ., which only involves three planes.

Since it is impossible to resolve the Si–C structure, the stacking sequence that it is observed in the micrograph must be that with the greatest number of planes in the repeating sequence, and hence that of Si. We enlarged each micrograph to be able to determine properly the stacking sequence of each atom row. Examining the stacking sequence on the right of the black arrow (Fig. 4b), in which the partial dislocation has not yet slipped, one observes that there is no change in the stacking sequence. In this region the SiC structure is 4H. However, on the left hand side, where the partial dislocation has slipped, one observes a change ACAB → BACA in the stacking fault (see the sequence shown in Fig. 4b).

3.2. Below the transition temperature

The dislocation microstructure below the transition temperature consists of partial dislocations originating from the dissociation process of Eq. (1). At this temperature (900 °C), one observes that the two partials do not glide together, but that only one of them glides in the basal plane. These results agree with those reported by Pirouz.[15] Nevertheless, the partial dislocations that are observed do not always have the same Burgers vector, as one sees in the inset of Fig. 5 in which, with $\boldsymbol{g} = 1\,1\,\bar{2}\,0$, only the dislocation number 5 is extinguished and therefore its Burgers vector is $\mathbf{b} = 1/3[1\,\bar{1}\,0\,0]$. This differs from Hong et al.[20] who observed the same Burgers vector for partial dislocations, and hence postulated a possible difference in the mobility between the leading and the trailing partials to explain that observation. They argued that the core of one partial would be richer in silicon, and its pair richer in carbon, leading to different activation barriers for nucleation, with the former having the greater mobility. The fact that we do not observe always de

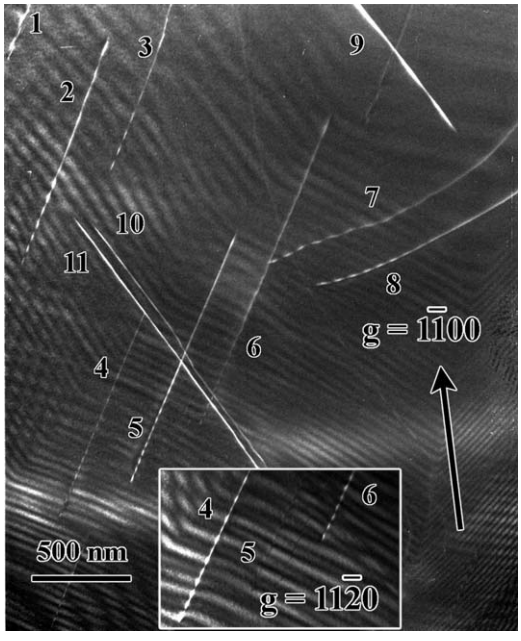

Fig. 5. TEM micrograph of a 4H–SiC specimen deformed by basal slip at 900 °C (1, 2, 6, 7, 8 have $\mathbf{b} = 1/3[0\,1\,\bar{1}\,0]$, 5, 9, 10, 11 $\mathbf{b} = 1/3[\bar{1}\,1\,0\,0]$, and 3, 4 $\mathbf{b} = 1/3[1\,0\,\bar{1}\,0]$).

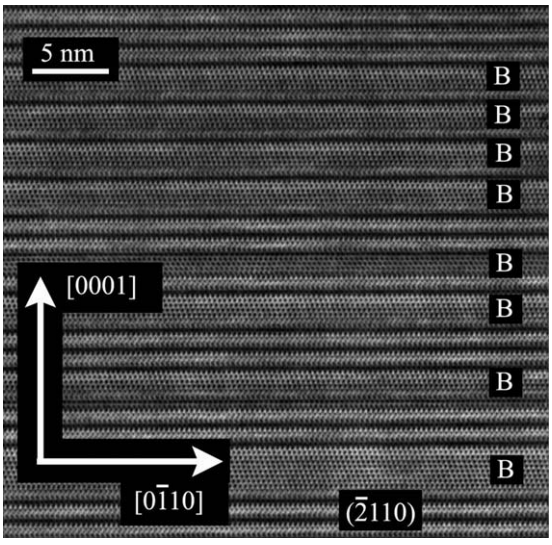

Fig. 6. High resolution micrograph of 4H–SiC deformed by basal slip at 900 °C, showing 3C bands (B).

same Burgers vector could be due to the activation of a secondary glide system, but this possibility is quite unlikely if we take into account that for one hand the orientation of specimens was selected to activate only one $(0\,0\,0\,1)1/3\langle\bar{1}2\bar{1}0\rangle$ basal slip system with a maximum Schmid factor ($f_s = 0.5$), and on the other hand dislocation densities are more or less the same for each $\mathbf{b} = 1/3\langle1\bar{1}00\rangle$.

Apart from the contour lines, one observes certain bands in the background of the micrograph. These are more clearly defined in the inset for $\boldsymbol{g} = 1\,1\,\bar{2}\,0$ conditions. These bands, absent in the micrographs of the specimen deformed at 1300 °C, might be related to the stacking fault produced in the material when only the leading partial dislocation slips.

High resolution micrographs of specimens deformed at 900 °C display clear differences from those deformed at 1300 °C. For instance, the different contrasts of 30 nm in length within the basal plane frequently found at 1300 °C are not present at 900 °C. Instead, there appear many bands (Fig. 6) whose nature will be discussed below.

At the top of Fig. 6, one observes pairs of planes with a dark contour, corresponding to the C and A silicon stacking plane sequence with clearly defined atom columns, followed

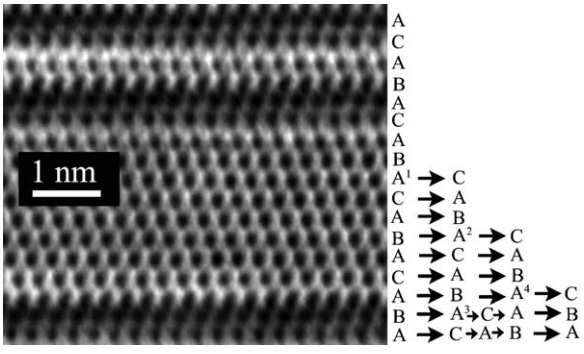

Fig. 7. Magnification of one band from Fig. 6 showing changes in the stacking plane sequence.

by pairs of planes with a brighter contour related to the B and A silicon stacking plane sequence with more poorly defined atom columns. The repetition of these two pairs of planes generates the 4H–SiC structure observed at the top and bottom of Fig. 6. Nevertheless, there are some bands (B in Fig. 6) in which this sequence is different. Micrograph 7 is a magnification of one of these bands. It corresponds to an analysis of the stacking plane sequence in the [0 0 0 1] direction. Starting from the top, and descending along the [0 0 0 1] direction, one finds the first change in the stacking sequence. This sequence should be "A^1", but instead it is "C". This change in the stacking plane sequence cannot take place after the glide of the two partial dislocations because the change of the stacking sequence produced after the glide of the leading partial is removed by the glide of the trailing partial. Instead, it can only can take place due to the glide of a $1/3\langle 1\,\bar{1}\,0\,0\rangle$ partial dislocation, which generates a region in which the part of the crystal below the slip plane is displaced with respect to the area above by a distance equivalent to the projection of its Burgers vector in the plane of observation.

One can thus imagine that between sequences "A^1" and "B" one leading partial has glided, producing a shift between the parts above and below. For simplicity, let us consider that the part above remains then same, it being the part below which has shifted. So now "A^1" is "C", and the stacking plane sequence of all the planes below is also changed after this shift, as is shown in the second column. Subsequently, this process could take place between sequences "A^2" and "B" and "A^3" and "B", generating the sequence described in the third column. Again, between "A^4" and "B" there occurs the glide of one partial, with the final stacking plane sequence shown to the right. The whole process finally gives rise to a 3C band in the 4H material. It should be emphasized that this band could be created by the glide of different partials as in "A^2" and "A^3", or by means of the cross-slip of a single given partial which probably occurs in "A^1" and "A^2".

3.3. Close to the transition temperature

The dislocation microstructure is quite similar in the specimens deformed at 1000 °C and 1100 °C. At these temperatures, there is a mixture of what was observed above and below the transition temperature (Fig. 8), with cases in which the two partial dislocations slip together after basal dissociation (D in Fig. 8), and cases in which the leading partial dislocation slips alone (L in Fig. 8). An example of the former case is seen in the top right inset of Fig. 8. This was taken using $\boldsymbol{g} = \bar{2}\,1\,1\,0$ reflection, and clearly shows the extinction of one partial – that with $\mathbf{b} = 1/3[0\,1\,\bar{1}\,0]$ – whereas its twin with $\mathbf{b} = 1/3[\bar{1}\,1\,0\,0]$ is visible. In the other two insets, also taken with $\boldsymbol{g} = \bar{2}\,1\,1\,0$, all dislocations of the area are extinguished, indicating that they all have the same Burgers vector ($\mathbf{b} = 1/3[0\,1\,\bar{1}\,0]$) and are slipping without their respective twins. The two mechanisms operate in the range 1100–1000 °C, so that the transition is not abrupt: while Demenet et al.[15] estimated its temperature as $T_c \approx 1030$ °C, there is a temperature range around T_c in which the two mechanisms coexist. According to our observations, this range lies within 1000–1100 °C. Furthermore, one or the other mechanism predominates depending on the temperature, since at higher temperatures there are far more partial pairs than leading partials slipping alone, while the situation becomes the contrary by decreasing temperature. It has to be emphasized that in the specimens deformed at both 1000 °C and 1100 °C one can again observe the sort of bands in the background of the micrograph which were observed in the specimens deformed at 900 °C but were absent at 1300 °C. They thus represent clear evidence for operation of the low temperature mechanism, as found in the specimens deformed at 900 °C.

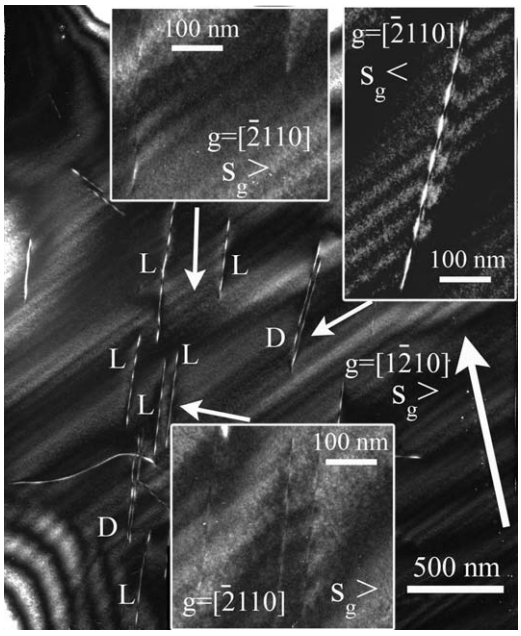

Fig. 8. Dislocation microstructure of 4H–SiC deformed by basal slip at 1000 °C.

Specimens deformed at temperatures close to the transition temperature were also studied by high resolution transmission electron microscopy. Since the weak beam-dark field imaging had shown the dislocation microstructure at these temperatures to be a mixture of what had been observed for temperatures above and below the transition temperature, it was to be expected that high resolution micrographs would also include elements of both regimes. Fig. 9 shows some bands of contrast different from the background (B in the figure) parallel to the basal plane and occupying the whole width of the images. These bands are typically observed in high resolution micrographs of specimens deformed below the transition temperature (Figs. 6 and 7). As we have shown, their structure is cubic.

Another type of different contrast is also observed (D in Fig. 9) which also lies in the basal plane but is much narrower – approximately 30 nm in width. These contrasts are observed in specimens deformed above the transition temperature (Fig. 4), and come from the stacking fault between partial dislocations. The dissociation width is approximately the same at 1300 °C as at 1100 °C, evidence that the stacking fault energy is constant in this range of temperatures.

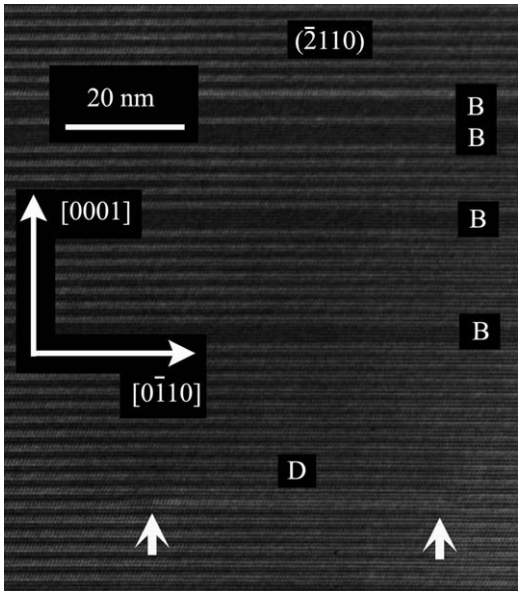

Fig. 9. High resolution micrograph of 4H–SiC deformed by basal slip at 1100 °C. 4-Cubic bands (B) and dissociation processes (D) are observed.

3.4. Correlation between dislocation microstructure and mechanical behaviour

The mechanical behaviour of 4H–SiC is characterized by two different regimes (see Fig. 1). In the low temperature regime, this material does not exhibit a clear and well marked yield point. Rather, after elastic deformation the material is quickly work hardened. At higher temperatures, however, the yield point is clearly observed, and work hardening is practically non-existent even for a large strain ($\varepsilon \sim 10\%$). These differences evidently reflect a change in the deformation mechanism. According to the literature, the mobility of a partial dislocation depends on the dislocation core, which in this case can be richer either in carbon or in silicon, with the latter having a greater mobility.[15] When the temperature is high enough to activate a self-diffusion process and the two partials can exchange point defects, then the difference in mobility is not significant and the two partial dislocations essentially slip together, as was seen in the micrographs of specimens deformed above the transition temperature. So the fact that Frank-Read sources are dissociated has no effect on its operation, and the yield point is expected because it is due to readjustments between the density of the dislocations, their speed, and the strain rate of the mechanical tests.

If, however, the temperature is not high enough then the trailing partial encounters serious difficulties in slipping together with the leading partial, which has far greater mobility. Finally, therefore, only the leading partial is emitted. Owing to the stacking fault generated by the partial glide, it is impossible for the same partial to be emitted again.[15] Moreover, after this single emission the situation is the reverse, i.e., the leading partial is now behind the trailing partial. Between the two partial dislocations there is a repulsive force that in the absence of stress would separate them by a distance d at which this force can no longer overcome the lattice friction. Nevertheless, the applied stress shortens this distance, thus increasing the energy of this configuration. There can be no cross-slip because the dislocations do not have a screw character. However, in order to reduce the energy, partial dislocations change slip plane by exchanging point defects in a self-diffusion process,[23] since bulk diffusion is negligible in SiC below about 1500 °C. In this process, the leading partial quickly gets ahead of the trailing partial. When they reach the adjacent basal plane, they again change slip plane in which to glide because the basal slip system is the most favoured. In this new basal plane, another leading partial could be emitted, generating a further stacking fault area in this basal plane. The repetition of this process generates the appearance of bands with cubic structure as were seen in Sections 3.2 and 3.3 above. Each source can emit only one leading partial in each basal plane, so the deformation of the material requires the partial dislocations to change successively the basal slip plane. This leads to a higher applied stress to maintain the strain rate of the mechanical test. Consequently, the material does not exhibit a yield point, and the elastic deformation is followed by a work hardening stage.

4. Conclusions

We have investigated the dislocation microstructure of 4H silicon carbide single crystals strained at around the transition temperature given in the literature – 1030 °C. Nonetheless, we investigated a far wider temperature range (from 900 °C to 1300 °C) which revealed that the two mechanisms coexist from 1000 °C to 1100 °C, meaning that the transition temperature is actually a range between, at most, these two temperatures. In the high temperature regime, WB-DF trace analyses using large-angle tilts showed that dissociation of basal dislocations takes place by glide, with partials being separated by 32 ± 4 nm. These results were corroborated by HRTEM observations. Consequently, we obtained a value for the stacking fault energy in the basal plane of $20 \pm 5\,\mathrm{mJ/m^2}$, which is in good agreement with the experimental and simulation results reported by various workers. Since the two partials slip together in the high temperature regime, glide dissociation has a negligible effect on mechanical properties. Dissociation of basal dislocations also takes place in the lower temperature regime, even at temperatures as low as 900 °C. However, in this regime the difference in mobility between the leading and the trailing partial seems to be so high that the latter cannot follow the former, which therefore glides alone. Hence, only the leading partials are observed in the micrographs. Nevertheless, we here found that not all the leading partials have the same Burgers vector, and also that they differ in character. This indicates that, not only the dislocation core composition as previously reported, but also the dislocation character strongly influence the dislocation mobility. Thus, the combination of the two factors finally decides which will be the leading and which the trailing partial after basal dissociation. This marked difference in mobility leads on the one hand to a different mechanical behaviour, characterized by rapid and strong work hardening, practically non-existent in the high temperature regime, and, on the other, to bands with 3C cubic structure within the 4H–SiC matrix in amounts that decrease with temperature, and to some special fringes in the WB micrographs which can also be taken as evidence for the operation of the low

temperature mechanism. From 1000 °C to 1100 °C, the dislocation microstructure is a mixture of the two configurations that we observed in the high and the low temperature regimes.

Acknowledgements

We are grateful to M. Kelsch and U. Salzberger for their help in TEM specimen preparation. This work was financially supported by the Ministry of Education and Science (Government of Spain) through the project MAT 2006-03068 and by the Junta de Andalucía (Spain) through the excellency project P05-0337-FQM.

References

1. Miao MS, Limpijumnong S, Lambrecht WRL. *Stacking fault band structure in 4H–SiC and its impact on electronic devices*. *Appl Phys Lett* 2001;**79**:4360–2.
2. Iwata H, Lindefelt U, Öberg S, Briddon PR. *Cubic polytype inclusions in 4H–SiC*. *J Appl Phys* 2003;**93**:1577–86.
3. Samant AV, Hong MH, Pirouz P. *The relationship between activation parameters and dislocation glide in 4H–SiC single crystals*. *Phys Status Solidi* 2000;**222**:75–93.
4. Pirouz P, Yang JW. *Polytypic transformations in SiC: the role of TEM*. *Ultramicroscopy* 1993;**51**:189–214.
5. Samant AV, Pirouz P. *Activation parameters for dislocation glide in* α*-SiC*. *Int J Refract Met H* 1998;**16**:277–89.
6. Fujita S, Maeda K, Hyodo S. *Dislocation glide motion in 6H–SiC single crystals subjecter to high-temperature deformation*. *Philos Mag A* 1987;**55**:203–15.
7. Ning XJ, Havey N, Pirouz P. *Dislocation cores and hardness polarity of 4H–SiC*. *J Am Ceram Soc* 1997;**80**:1645–52.
8. Rabier J, George A. *Dislocations and plasticity in semiconductors. II – the relation between dislocation dynamics and plastic deformation*. *Rev Phys Appl* 1987;**22**:1327–51.
9. Pirouz P, Samant AV, Hong MH, Moulin A, Kubin LP. *On temperature dependence of deformation mechanism and the brittle–ductile transition in semiconductors*. *J Mater Res* 1999;**14**:2783–93.
10. Lagerlöf KPD, Castaing J, Pirouz P, Heuer AH. *Nucleation and growth of deformation twins: a perspective based on the double-cross-slip mechanism of deformation twinning*. *Philos Mag A* 2002;**82**:2841–54.
11. Zhang M, Hobgood HM, Demenet JL, Pirouz P. *Transition from brittle fracture to ductile behavior in 4H–SiC*. *J Mater Rev* 2003;**18**:1087–95.
12. Okojie RS, Xhang Ming, Pirouz P, Tumakha S, Jessen G, Brillson LJ. *Observation of 4H–SiC to 3C–SiC polytypic transformation during oxidation*. *Appl Phys Lett* 2001;**79**:3056–8.
13. Kuhr TA, Liu J, Chung HJ, Skowronski M, Szmulowicz F. *Spontaneous formation of stacking faults in highly doped 4H–SiC during annealing*. *J Appl Phys* 2002;**92**:5863–72.
14. Idrissi H, Lancin M, Douin J, Regula G, Pichaud B. *Dynamical study of dislocations and 4H to 3C transformation induced by stress in 4H–SiC*. *Mater Sci Forum* 2005;**299**:483–5.
15. Demenet JL, Hong MH, Pirouz P. *Plastic behaviour of 4H–SiC single crystals deformed at low strain rates*. *Scripta Mater* 2000;**43**:865–70.
16. Castillo-Rodríguez M, Castaing J, Muñoz A, Veyssière P, Domínguez-Rodríguez A. α*-Al_2O_3 sapphire and rubies deformed by dual basal slip at intermediate temperatures (900–1300 °C) II. Dissociation and stacking faults*. *Acta Mater* 2009;**57**:2879–86.
17. Hirth JP, Lothe J. Theory of Dislocations. New York: McGraw Hill; 1968.
18. Umeno Y, Cerný M. *Effect of normal stress on the ideal shear strength in covalent crystals*. *Phys Rev B* 2008;**77**:100101–4.
19. Hong MH, Samant AV, Orlov V, Farber B, Kisielowski C, Pirouz P. Deformation-induced dislocations in 4H–SiC and GaN. In: *Mater Res Soc Symp Proc*. 1999.
20. Hong MH, Samant AV, Pirouz P. *Stacking fault energy of 6H–SiC and 4H–SiC single crystals*. *Philos Mag A* 2000;**80**:919–35.
21. Käckell P, Wenzien B, Bechstedft F. *Influence of atomic relaxations on the structural properties of SiC polytypes from ab initio calculations*. *Phys Rev B* 1994;**50**:17036–7.
22. Cheng C, Needs RJ, Heine V. *Inter-layer interactions and the origin of SiC polytypes*. *J Phy C* 1988;**21**:1049–63.
23. Pirouz P, Hazzledine PM. *Cross-slip and twinning in semiconductors*. *Scripta Metall Mater* 1991;**25**:1167–72.